ACS OMEGA

http://pubs.acs.org/journal/acsodf

Article

Green Synthesis of Nano-Zero-Valent Iron Using *Ricinus Communis* Seeds Extract: Characterization and Application in the Treatment of Methylene Blue-Polluted Water

Ahmed M. Abdelfatah, Manal Fawzy, Abdelazeem S. Eltaweil,* and Mohamed E. El-Khouly*

Cite This: *ACS Omega* 2021, 6, 25397−25411

Read Online

ACCESS | Metrics & More | Article Recommendations

ABSTRACT: In this study, the removal of methylene blue dye (MB) from aqueous solution was examined using a novel green adsorbent to overcome the obstacles encountered in chemical methods. *Ricinus communis* (RC) aqueous seeds extract was herein used as a reducing and capping agent to synthesize a novel nano-zero-valent iron (RC-nZVI) for the adsorption of harmful MB. Structural and morphological characterization of the synthesized RC-nZVI were performed using several techniques, e.g., steady-state absorption, scanning electron microscopy (SEM), transmission electron microscopy (TEM), Fourier transform infrared (FT-IR), energy-dispersive X-ray spectroscopy (EDS), X-ray diffraction (XRD), X-ray photoelectron spectroscopy (XPS), and zeta potential. The maximum efficiency of the removal was 96.8% at pH 6 and 25 °C. According to the kinetics study results, the adsorption process obeys the pseudo-first-order model. The experimental equilibrium data were fitted to the Freundlich isotherm model, the maximum adsorption capacity reached was 61.37 mg·g^{-1}, and the equilibrium parameters were determined. The synthesized RC-nZVI possesses good reusability and can be considered as a potential economic and environmentally friendly adsorbent.

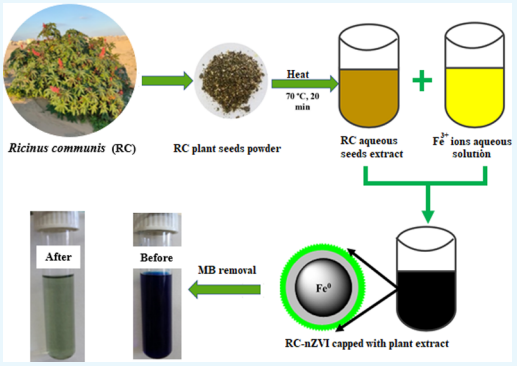

1. INTRODUCTION

There is no doubt that water is a vital resource for all creatures, and its treatment is a must nowadays due to the augmentation of water pollution with various pollutants. Nitroaromatic compounds, chlorinated compounds, dyes, heavy metals, and anthropogenic chemicals are the most harmful categories of pollutants that need to be removed from the aquatic environment.[1,2] Different manufacturing applications that use dye compounds, such as food, textiles, cosmetics, and paper industries, discharge thousands of tons of dye effluents annually.[3,4] Organic pollutants, notably aromatic compounds with a benzene ring structure, have a more stable structure, are difficult to decompose, and are highly toxic, resulting in serious pollution of the environment.[5−7] Among the most harmful pollutants, methylene blue (MB) is one of the most commonly used cationic dye; however, its discharge can cause kidney, brain, liver, and central nervous system deterioration.[8,9] Owing to its complex chemical structure, MB is nonbiodegradable and can adversely affect aquatic ecosystems by preventing the penetration of sunlight into water and streams.[10−12] In addition, MB can inhibit microorganisms' catalytic activity, contributing to their death, which can cause severe health problems, such as vomiting, nausea, diarrhea, and stomach upset.[13]

Recently, the removal of these organic pollutants has been a major concern, due to their deleterious effects. Diverse physical, chemical, biological, and electrochemical processes have been used to treat these pollutants from wastewater.[14−16] Catalytic degradation is one of the main routes for the removal of these dyes.[17,18] Advanced oxidation processes, another effective way for the removal of dyes, is mainly concerned with the formation of hydroxyl radicals (•OH) that readily oxidize these dyes into H_2O, CO_2, and other nontoxic small molecules.[19,20] Among the used techniques, adsorption has been recognized as a favorable one due to its high efficiency and relatively low cost of energy and capital expenditure.[16,21−24]

Green synthesis of nanomaterials represents a key solution to overcome the unfavorable impacts of their production via chemical routes.[25,26] Green synthesis of nanoparticles should be widely used in real life and moved beyond the laboratory owing to its unique features, e.g., environmentally friendly,

Received: June 27, 2021
Published: September 23, 2021

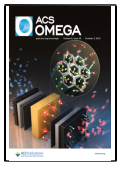

nontoxic, and safe. Among the green-synthesized nanoparticles, nano-zero-valent iron (nZVI) has attracted great attention in industrial and environmental applications[27] due to its unique properties, e.g., small size, large specific surface area, high interfacial reactivity, and high magnetic nature.[28,29] The unique structural and electronic properties of the synthesized nZVI make it a promising material for removing the toxic pollutants from contaminated water, such as heavy metals,[30,31] antibiotics,[32] chloroorganics,[33] bromides,[34] nitrates,[34] dye pollutants,[29,35] and cesium.[36]

Compared to the ease of fabrication, low cost, and environmentally friendly nature of the green-synthesized nZVI, the traditional chemical methods used for the synthesis of nZVI are still facing many problems such as hazardous byproducts generated by precursors and solvents, the contamination resulting from use of harmful chemical compounds, as well as low production rates and high energy consumption.[37−39] In addition, the strong magnetic forces in nZVI usually lead to aggregation of particles, which has been the main impediment to its practical application.[40] The surface modification of nZVI with dispersants has been extensively studied, which proved to be a viable approach to promoting the stability and fluidity of nZVI in the ambient medium.[41,42] Nonbiodegradable dispersants, however, are generally considered to have significant toxicity and could cause secondary contamination if used on a large scale. Therefore, alternative methods of low cost and green synthesis are urgently required. The reduction of ferric or ferrous iron using bioactive substances derived from plant extracts has received extensive attention as one of the nZVI synthesis alternatives.[43] Plant extracts can be used as a highly effective and environmentally sustainable alternative for the synthesis of nanoparticles, instead of physiochemical methods, which have less energy efficiency (require high temperature and pressure). Besides, the abundance and easy availability of plants make them a significant candidate for biogenic synthesis.[44,45] Various plant extracts have been reported in the green synthesis of nZVI, including the leaf extract of *Mangifera indica*, pomegranate peel extract, *Thymus vulgaris*, *Urtica dioica*, and *Rosa damascene*.[46−48] *Ricinus communis* belongs to the family *Euphorbiaceae*, which is a monotypic genus, and is found throughout the country and is widely cultivated in the tropics and warm regions for its seeds, which yield the well-known castor oil. Experimental and clinical studies demonstrate that *R. communis* has a wider spectrum of pharmacological and therapeutic effects.[49]

To the best of our knowledge, green synthesis of nZVI using castor oil (*R. communis*) is rare in the literature. Taking the advantages of green synthesis and the unique properties of nZVI into consideration, we report herein the green synthesis of nZVI using *R. communis* seeds extract as a reducing and stabilizing agent, and characterization of the synthesized nZVI using various spectroscopic and analytical techniques, and evaluate the potentiality of the synthesized nZVI for the removal of cationic methylene blue dye (MB).

2. RESULTS AND DISCUSSION

2.1. Phytochemical Screening of *R. communis*. The phytocomponents of plant extract act as a reducing as well as stabilizing agent. However, the basic mechanism of phytosynthesis of MNPs has not been well understood, and various putative mechanisms have been proposed for their synthesis.[50−52] It is a tedious process to identify any specific bioreducing and stabilizing mediators responsible for the synthesis and stabilization of MNPs due to the complex nature of phytochemicals in plant extracts. To date, phytocomponents including polyphenols (flavonoids, phenolic acid, and terpenoids), or organic acids, and proteins are considered as possible bioreducing and stabilizing agents for the synthesis of MNPs.[53,54] So, in the present study, a preliminary phytochemical screening of some bioactive compounds of *R. communis* was carried out using suitable chemical reagents to indicate the presence or absence of the chemical constituents that are usually involved in the phytosynthesis of Fe^0. The test results indicated the presence of high contents of tannins, alkaloids, fats and fixed oils, and phenols, a moderate content of saponins and carbohydrates, and low contents of anthraquinone glycosides as presented in Table 1. This variety in the phytochemical compounds provides strong reducing properties that mediate the synthesis of nZVI through the reduction of Fe^{3+} ions.

Table 1. Qualitative Phytochemical Screening for the Aqueous Extract of RC Seeds[a]

no	test name	phytochemical compound	result
1	Ferric chloride test	tannins	+++
2	Dragendorff's test	alkaloids	+++
3	Foam test	saponins	++
5	Alkaline reagent test	flavonoids	+++
6	Molisch's test	carbohydrates	++
7	Potassium ferricyanide test	phenols	+++
8	Copper sulfate test	fats and fixed oils	+++
9	Hydroxyanthraquinone test	anthraquinone glycosides	+

[a](+++) = high amount [appears immediately after addition of reagent]; (++) = moderate amount [appears after 5 min of reagent addition]; (+) = low amount [appears after 10 min of reagent addition]; and (−) = absence of active compound [not detected after 20 min].

2.2. Characterization of RC-nZVI Nanoparticles. *2.2.1. UV−vis Spectral Analysis and Effect of Incubation Time.* The reduction of Fe^{3+} to nZVI was confirmed by the visible color change in the reaction mixture, serving as a preliminary indication of the formation of nZVI.[55] In the current study, an immediate change in the solution color from reddish brown to black at room temperature was detected after the addition of the plant seeds extract, indicating the rapid synthesis of RC-nZVI (Figure 1A). It was reported that the formation of the dark color of the synthesized nZVI is basically due to the complexation of Fe^{3+} with the phenolic group in the plant extract as a metal−ligand interaction between Fe^0 and the polyphenolic compound via the C═O bond.[56−58] The pH of the plant extract was found to be 5.2; however, after adding it to the Fe^{3+} ions solution, the pH dropped to 2.25, which could be due to the generation of H^+ during the reduction of Fe^{3+} by polyphenols or other reducing agents present in plant extracts, as shown in the reaction below.[59]

$$n\mathrm{Fe}^{3+} + 2\mathrm{Ar} - (\mathrm{OH})_n - n\mathrm{Fe}^0 + 3n\mathrm{Ar} = \mathrm{O} + 3n\mathrm{H}^+$$

where n is the number of hydroxyl groups oxidized by Fe^{3+}, and Ar stands for the polyphenol group.

UV−vis absorption spectra for the Fe^{3+} ions aqueous solution, RC seed extract, and the synthesized RC-nZVI are represented in Figure 1A. The absorption spectrum of RC-nZVI exhibited a maximum in the range of 216−300 nm,

https://doi.org/10.1021/acsomega.1c03355
ACS Omega 2021, 6, 25397−25411

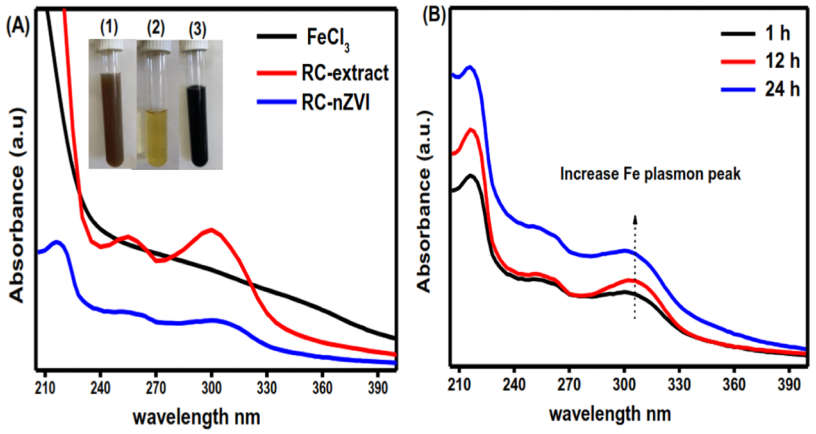

Figure 1. (A) UV−visible absorption spectra of an aqueous solution of Fe^{3+} ions, RC seed extract, and synthesized RC-nZVI. (B) UV−visible absorption spectra of the synthesized RC-nZVI at different incubation times.

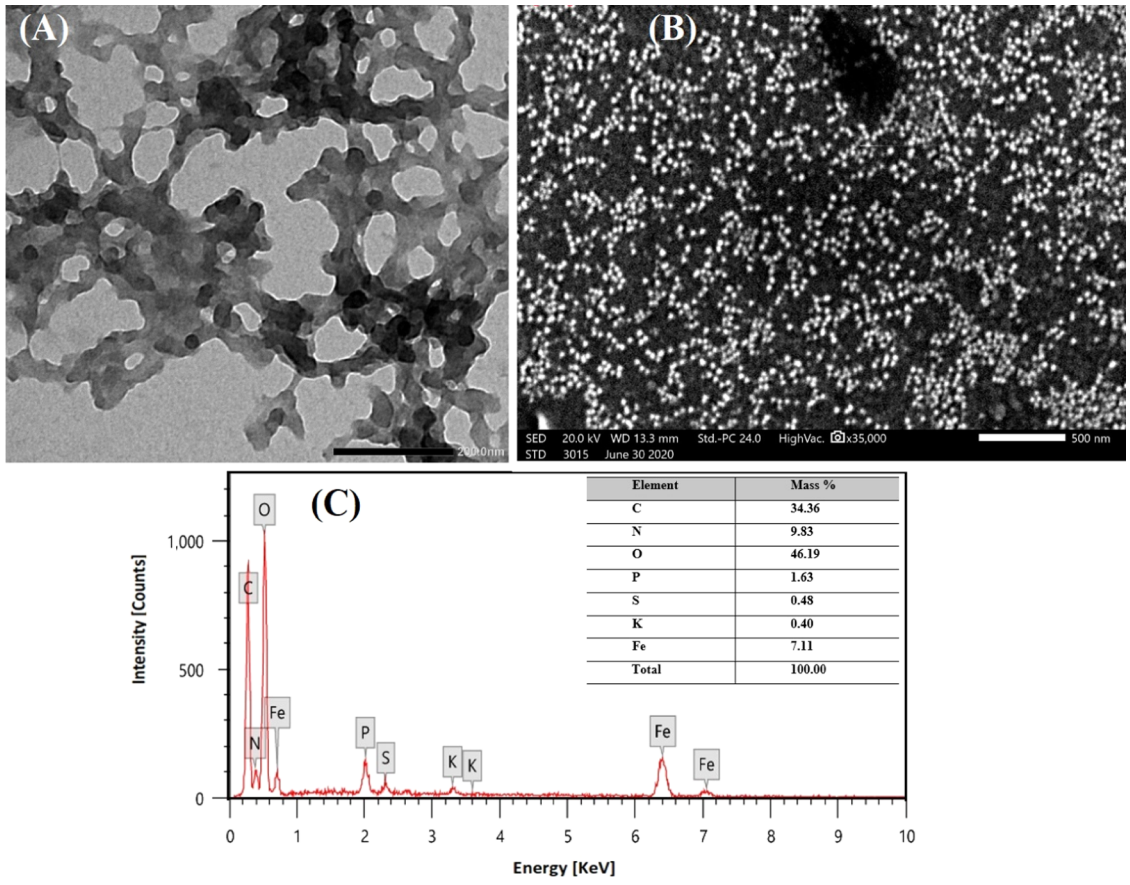

Figure 2. SEM images (A, B), TEM images (C, D), and EDX pattern of RC-nZVI (E).

which is identical to the characteristic absorption peak for the reported metallic iron.[60] These results are in good agreement with a previously published work by Pattanayak and Nayak,[61] where nZVI was synthesized using *Azadirachta indica* with an absorption peak for nZVI in the wavelength range 216−268 nm. Furthermore, Somchaidee and Tedsree[62] recorded the absorption peaks for the phytosynthesized nZVI using guava (*Psidium guajava* L) leaf extract at 200−300 nm. In addition, Eslami et al.[63] reported the absorption bands of the aqueous extract of *Myrtus communis* leaves and the development of the nZVI at 260 and 210 nm, which are considered the signature bands for nZVI.

The effect of incubation time on the green synthesis process is another important factor that greatly affects the characteristics of nZVI. On this account, the UV−vis spectra of the synthesized nZVI were monitored at different time intervals of 1, 12, and 24 h. The UV−vis spectra of the synthesized nZVI using RC seed extract showed an increase in intensity with time as shown in Figure 1B. This may arise from the excitation of longitudinal plasmon vibrations in MNPs in the solution, reflecting the continued reduction of the synthesized nZVI.[64]

2.2.2. Electron Microscopy Analysis. Transmission electron microscopy (TEM) and scanning electron microscopy (SEM) were carried out to understand the particle size, shape,

https://doi.org/10.1021/acsomega.1c03355
ACS Omega 2021, 6, 25397−25411

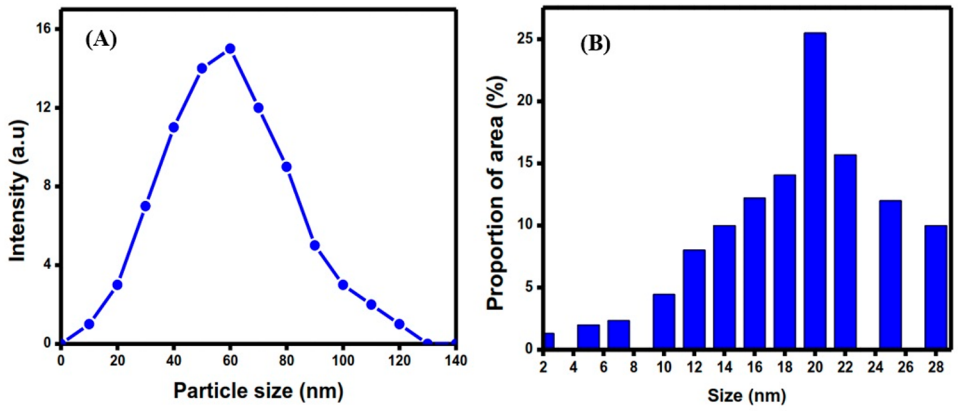

Figure 3. (A) DLS of the size distribution and (B) TEM micrograph of the particle size distribution.

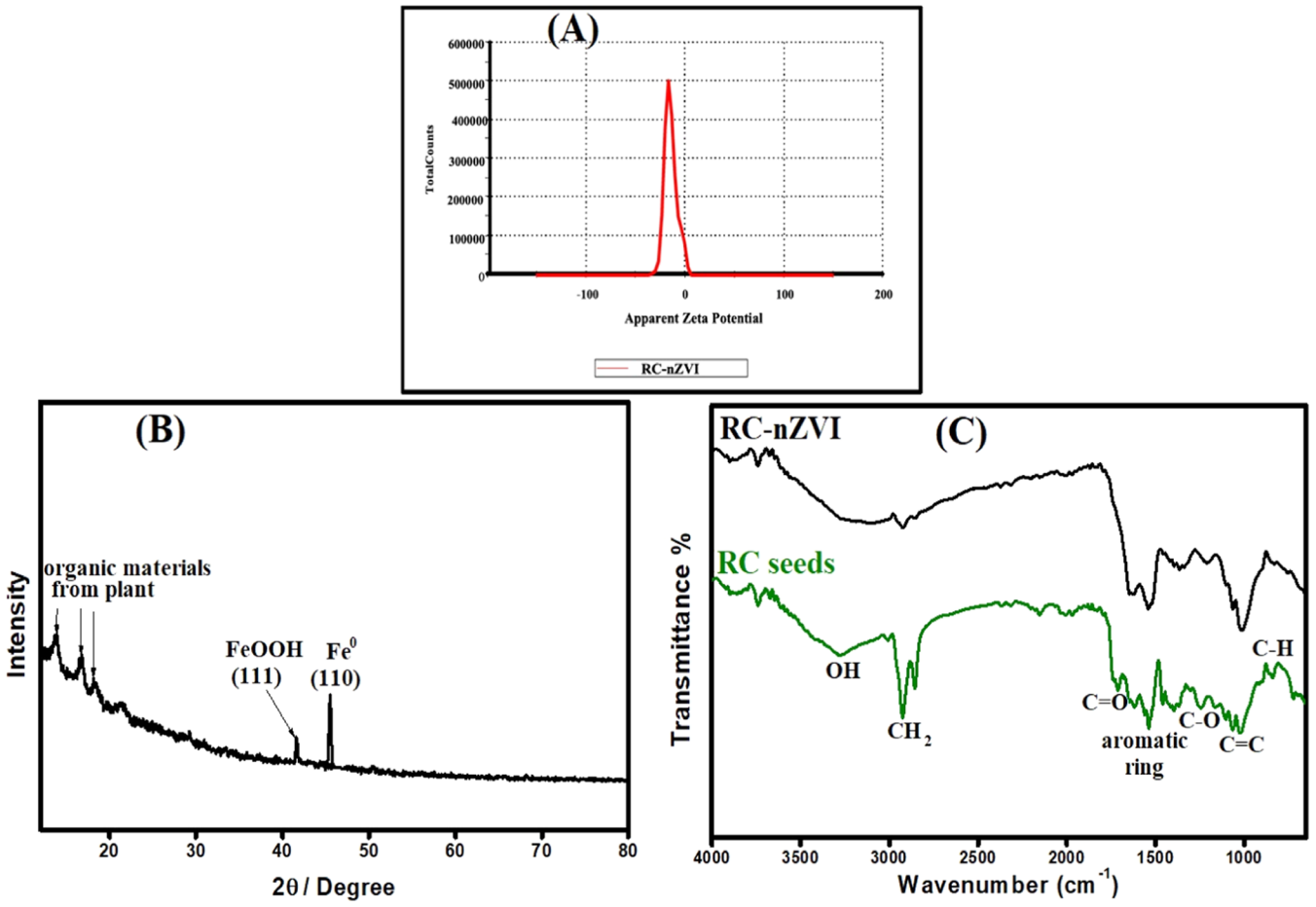

Figure 4. ζ-potential (A) and X-ray diffraction (XRD) (B) of RC-nZVI and Fourier transform infrared (FT-IR) spectra for both RC seeds and RC-nZVI (C).

dispersity, and topology of the synthesized RC-nZVI. From TEM images (Figure 2A), it can be seen that RC-nZVI exhibited a spherical shape along with some irregular shapes and has a tendency to form chain-like aggregates with an average particle size of 20 nm. The nanoscale particle size in the chain provides its high specific surface area and reactivity with contaminants.[65] Furthermore, the surface of the synthesized RC-nZVI is covered by a transparent layer, as demonstrated by the TEM images, which serves as a capping and stabilizing agent to prevent RC-nZVI from agglomerating and plays a crucial role in improving its dispersion and stability as a basic constituent of green-synthesized nZVI.[57,66,67] In the current investigation, SEM images added more support to those of TEM and confirmed that the synthesized RC-nZVI was mostly granular with a spherical shape, as shown in Figure 2B. In addition, the EDX analysis was performed to investigate the elemental composition of the synthesized RC-nZVI. As observed from Figure 2C, Fe, C, and O peaks confirm the formation of RC-nZVI. Moreover, the Fe, C, and O contents were found to be 7.11, 34.36, and 46.16%, respectively. These findings were in line with other works that reported the green

https://doi.org/10.1021/acsomega.1c03355
ACS Omega 2021, 6, 25397−25411

synthesis of nZVI using tea and Eucalyptus leaf plant extracts.[68,69]

2.2.3. Dynamic Light Scattering (DLS) Analysis and Size Distribution. Dynamic light scattering (DLS) has been utilized to investigate the aggregation phenomena of FeNPs in solution.[70] The final colloidal state and its evolution in terms of aggregation, reaction, and core−shell formation are all influenced by the metal colloid's synthesis. In this study, the average size of RC-nZVI was determined through DLS (Figure 3A). Results indicated that the size distribution of RC-nZVI in aqueous solution lies between 40 and 50 nm. However, the variation of size distribution and mean size of RC-nZVI obtained from the TEM photomicrograph (Figure 3C) indicated that the size distribution of the particle lies between 10 and 30 nm and the highest frequency of the particle size is 20 nm.

2.2.4. ζ-Potential (ZP). The ability to measure the ζ-potential of nanoparticles in dilute concentrations is a useful tool in a variety of fields. This parameter, for example, could be used in the nanotoxicological community to predict the environmental impact of commercial nanoparticles as well as their effects on human health. As a result, the ζ-potential can be used as a base for analyzing specific regulatory end points in relation to nanoparticle safety.[71] Additionally, the ζ-potential (ZP) was used for determining the degree of electrostatic attraction or repulsion between particles in a liquid suspension. On this basis, ZP is one of the main tools that measure the stability of nanoparticles in an aqueous solution. In the absence of steric stabilization, particles with ζ-potentials greater than +30 mV and less than −30 mV are considered stable for colloidal dispersion.[72] The recorded ζ-potential for the synthesized RC-nZVI is −14.9 mV, as shown in Figure 4A and Table 2. Accordingly, the synthesized RC-nZVI acquires a stable dispersal potential in the solution than the uncoated nanoparticles (−2.43 mV).[73] These negative charges on its surface suggest that RC-nZVI is a potential adsorbent for cationic dyes.

Table 2. ζ-Potential Parameters and Deviation Values

		mean (mV)	area (%)	st dev (mV)
ζ-potential (mV)	−14.9	peak 1: −14.9	100.0	4.41
ζ-deviation (mV)	4.31	peak 2: 0.00	0.0	0.00
conductivity (mS cm^{-1})	0.340	peak 3: 0.00	0.0	0.00
result quality	good			

2.2.5. XRD Pattern. The XRD pattern of RC-nZVI (Figure 4B) showed that the pattern of the synthesized RC-nZVI acquired a diffraction peak with high intensities at 2θ = 41.7° corresponding to the (111) plane of α-FeOOH. This is due to the shell layer of zero-valent iron nanoparticles as reported by Li et al.[74] They explained that nZVI is composed of the core (metallic iron) and the shell, i.e., the oxide layer of Fe(II) and Fe(III), which is formed due to the rapid metallic iron oxidation in the environment. However, the strong peak at 44.5° corresponding to the (110) plane represents Fe^0 (110). This characteristic peak at 2θ = 44.5° is attributed to the cubic phase structure of nZVI according to JCPDS card, No. 06−0696.[75] These results confirm the successful formation of nZVI. The presence of only one peak for the nZVI in the XRD pattern may be due to the high background caused by the X-ray florescence of Fe. When performing XRD of materials containing elements such as Fe and Mn, the secondary X-ray emitted by the elements causes high background levels that ruin the pattern. Increasing the scanning time slightly improves the quality of the diffraction pattern. Moreover, the three different peaks at 2θ = 13.81, 16.86, and 18.49° are attributed to the organic matter on the surface of the RC-nZVI.[14] The presence of these diffraction peaks confirms the fundamental role of the RC seed extract in the bioreduction and stabilization of nZVI.[41]

2.2.6. FT-IR Analysis. FT-IR spectra provide information about the surface structures and functional characteristic groups responsible for the reduction and stabilization of the green-synthesized RC-nZVI. The FT-IR spectra for the RC seed extract and RC-nZVI are shown in Figure 4C. For the RC seed extract, the peak at 3285 cm^{-1} is assigned to the characteristic O−H stretching vibrations in H_2O molecules, as well as the O−H groups of polyphenols in the RC seeds.[43,76] The peak at 2919 cm^{-1} is corresponding to the C−H and CH_2 vibrations of aliphatic hydrocarbons.[77,78] The peak at 1735 cm^{-1} is attributed to the C═O stretching vibration of the carbonyl group derived from the RC seeds.[68] The absorption peak at 1534 cm^{-1} is associated to the aromatic ring stretching vibration in the phenolic compound. The peak located at 1252

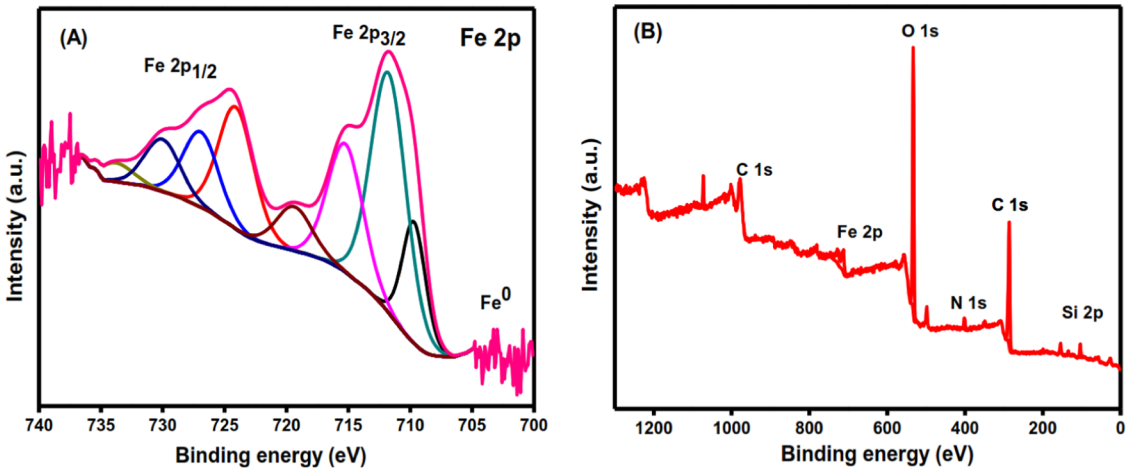

Figure 5. (A) XPS spectra for Fe 2p, and (B) wide spectrum of RC-nZVI.

https://doi.org/10.1021/acsomega.1c03355
ACS Omega 2021, 6, 25397−25411

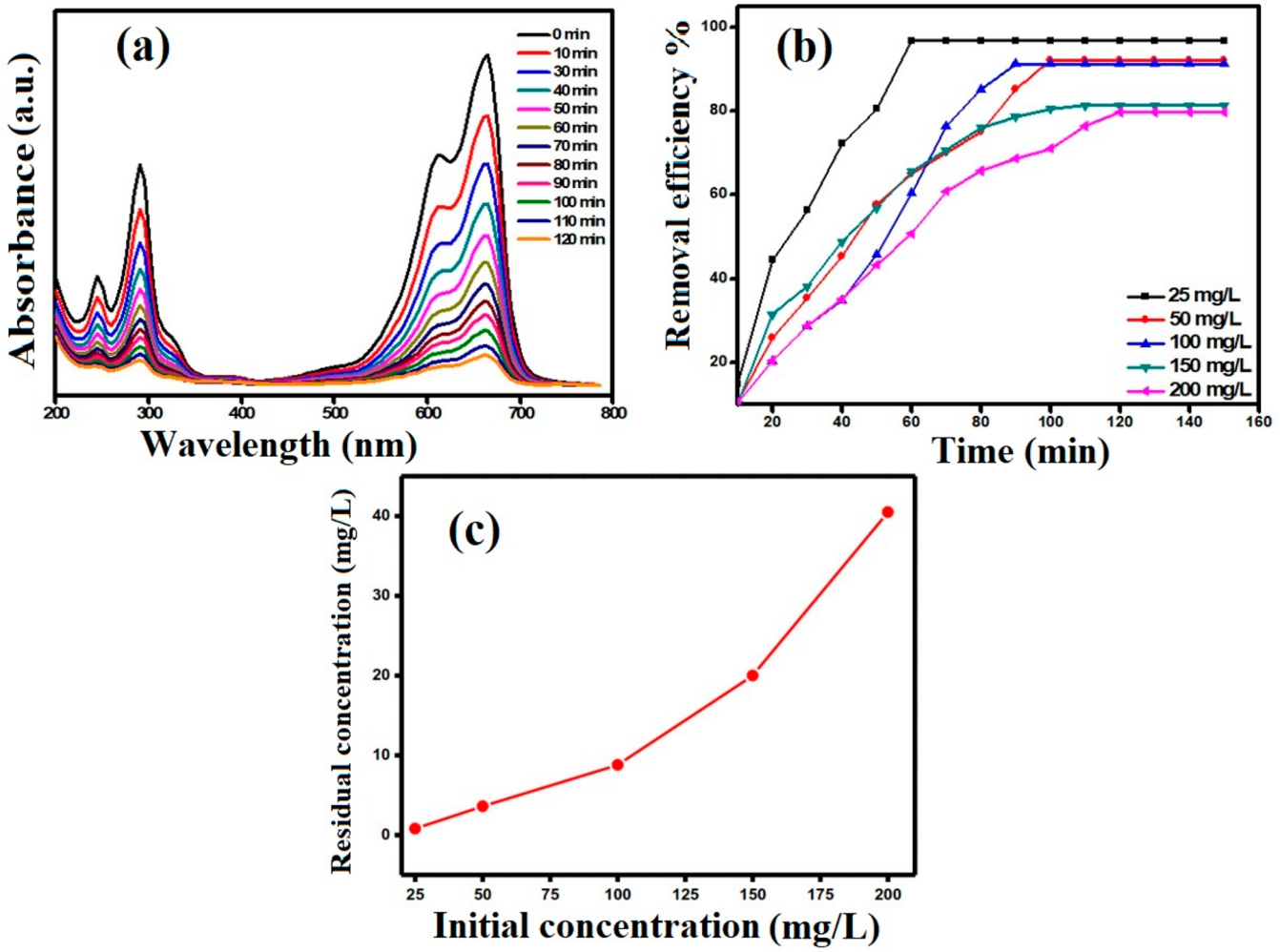

Figure 6. (a) UV−vis absorption spectra [C_o = 200 mg·L^{-1}, m = 30 mg, pH = 6, V= 10 mL], (b) q_t versus contact time, and (c) initial versus residual concentration for the removal of MB onto RC-nZVI.

cm^{-1} is assigned to C−O, C−O−H, and symmetric and asymmetric C−O−C groups.[79,80] Furthermore, the FT-IR spectrum of RC-nZVI shows the main characteristic peaks well matching that of the RC seeds, indicating that the nZVI surface is covered with active ingredients of RC seeds.

2.2.7. XPS Analysis. XPS is the most sensitive and widely used technique for determining the exact elemental ratio and bonding nature of the elements in NP materials. It is a surface-sensitive technique that can be used in depth-profiling studies to determine the overall composition and variation in composition with depth.[81] The wide XPS spectrum of RC-nZVI showed three peaks at 709.69, 724, and 726 eV (Figure 5A), representing the binding energies of Fe ($2p_{3/2}$) and shake-up satellite ($2p_{3/2}$ and $2p_{1/2}$) peaks, which confirm the existence of Fe(II) and Fe(III). The small peak at 704 eV is related to the $2p_{3/2}$ peak of nZVI.[82] This peak is expected to be small in XPS since it is a surface analysis and the nZVI surface is largely made up of oxides. The co-existence of a small fraction of Fe^0 compared to that of iron oxides confirms the core−shell structure of nZVI.[83] The main composition of RC-nZVI is carbon, oxygen, nitrogen, and silicon, as shown in Figure 5B, which was previously confirmed by the EDX analysis (Figure 2C).

2.3. Study of MB Removal. *2.3.1. Adsorption Kinetics Studies.* Figure 6A represents the UV−vis spectrum for the decrease in absorbance of MB (200 mg·L^{-1}) with contact time in the presence of RC-nZVI (30 mg). The impact of variation of MB concentration on the adsorption was analyzed by taking different concentrations (25−200 mg·L^{-1}) with a fixed quantity of RC-nZVI (30 mg) while the pH was adjusted at 6. It was observed that the percentage removal of MB decreases with the increase in initial concentration of the MB dye. The removal efficiency decreases from 96.8 to 79.75% as the initial concentration increases from 25 to 200 mg·L^{-1}. The increase in loading capacity of the adsorbent concerning dye ions is probably due to a high driving force for mass transfer. The more concentrated the solution, the better the adsorption capacities. As seen from Figure 6B, the adsorption capacities of RC-nZVI increase from 8.1 to 53.16 mg·g^{-1}. The concentrations of MB before and after adsorption onto RC-nZVI are shown in Figure 6C.

Adsorption kinetics study is a useful method to evaluate the dye adsorption performance, which is necessary to evaluate the dye adsorption efficiency. Hence, different kinetic models were applied on the experimental data of the adsorption of MB onto RC-nZVI, including pseudo-first-order, pseudo-second-order, and Elovich models. Table 3 lists the linear forms of these kinetic equations.

The results obtained from these models indicated that the adsorption of MB onto RC-nZVI follows the pseudo-first-order

https://doi.org/10.1021/acsomega.1c03355
ACS Omega 2021, 6, 25397−25411

Table 3. Kinetic Models and Adsorption Isotherms Used in the Present Study[a]

	model	linear form
kinetic models	pseudo-first-order	$\ln(q_e - q_t) = \ln q_e - K_1 t$
	pseudo-second-order	$\frac{1}{K_2 x q_e^2} + \frac{1}{q_e}$
	Elovich	$\ln(\alpha\beta) + 1/\beta \ln(t)$
	goodness of adsorption (Chi-square)	$\chi^2 = \sum \frac{(q_{e,exp} - q_{e,cal})^2}{q_{e,cal}}$
adsorption isotherm	Langmuir isotherm	$C_e/q_e = 1/K_L q_{max} + C_e/q_{max}$ $R_L = \frac{1}{1 + K_l C_o}$
	Freundlich isotherm	$\log(q_e) = \log(K_f) + \frac{1}{n}\log(C_e)$
	Temkin	$q_e = B_1 \log A + B_1 \log C_e$

[a] q_e, q_t, and q_m are the amount of adsorbed dye at equilibrium, the amount of dye adsorbed at time t, and the maximum adsorption capacity ($mg \cdot g^{-1}$), respectively. K_1 and K_2 are the rate constant of pseudo-first-order (min^{-1}) and rate constant of pseudo-second-order ($g \cdot mg^{-1} \cdot min^{-1}$), respectively. β is the desorption constant ($g \cdot mg^{-1}$) and α is the initial adsorption rate ($mg \cdot g^{-1} \cdot min^{-1}$). C_e is the equilibrium concentration ($mg \cdot L^{-1}$), K_L is the adsorption equilibrium constant ($L \cdot mg^{-1}$), R_L is the separation factor, B_1 is the Temkin constant, and A is the equilibrium bond constant.

kinetic model, where the R^2 value obtained from this kinetic model ($R^2 > 0.97$) were found to be higher than those of the other two models (Table 4 and Figure 7), thus confirming that this kinetic model better describes the MB adsorption onto RC-nZVI. In addition, the calculated values of ($q_{e,cal}$) were found to be in good agreement with the experimental ones ($q_{e,exp}$). Furthermore, K_1 values decrease with increase in the initial concentration of MB dye, revealing that the adsorption of MB by RC-nZVI is a physical adsorption reaction. The removal of MB by biowaste granules also fitted to pseudo-first-order in a study performed by Jaiyeola et al.[84] and another study performed by Sahu et al.[85] They found that the adsorption of MB onto nZVI follows the pseudo-first-order kinetic model. The Elovich model effectively describes the interaction between a solid and liquid interface, and takes into account that the real solid surface is energetically heterogeneous and that the desorption process and interactions between adsorbed species have little effect on the adsorption kinetics.[86] As it can be seen from Table 4, the value of α is higher than that of β for MB, which indicates a low desorption rate and a higher adsorption rate, implying that MB has an effective tendency to be adsorbed onto RC-nZVI.[87]

The chi-square (χ^2) test is used to assess the difference between the experimental and model data. If the model's data match the experimental data, χ^2 will be a small value, but if they do not, χ^2 will be a high value.[88] According to the results obtained from the model, the χ^2 values for the pseudo-first-order were 0.944 and 34.529. Thus, the lower χ^2 value for the pseudo-first-order suggests that MB dye adsorption onto RC-nZVI follows pseudo-first-order; the value of pseudo-second-order suggests poor fitting to the data for MB adsorption onto RC-nZVI.

2.3.2. Adsorption Isotherm Models. Adsorption isotherms play an essential part in describing the interaction between the adsorbate and the adsorbent at equilibrium. Therefore, the adsorption isotherm study is an important step in the designing of the adsorption system.[89] In this study, the equilibrium data for adsorption of MB onto RC-nZVI were analyzed by different isotherm models, including Langmuir, Freundlich, and Temkin models. This information can provide the relationship between the adsorbate and absorbent, in which the surface and adsorbate might adhere via chemisorption or physisorption.[90] The linear forms of these models are summarized in Table 3. It is clear from the isotherm plots (Figure 8) and the derived parameters (Table 5) that the adsorption of MB dye onto RC-nZVI is fitted to the Freundlich model ($R^2 = 0.990$). Therefore, the MB molecules were adsorbed on the film surface by way of multilayer adsorption. The derived n value is greater than 1 (1.838), indicating moderate adsorption intensity of MB onto RC-nZVI. Moreover, the maximum adsorption capacity (q_{max}) calculated from Langmuir was 61.73 $mg \cdot g^{-1}$. Moreover, the dimensionless constant separation factor (R_L) used at different initial concentrations of the MB dye lies between 0 and 1, which signifies that the adsorption of RC-nZVI is favorable. In the literature, a similar isotherm model fitting has been obtained for the adsorption isotherms of various pollutants onto different adsorbents.[13,91,92] The linear plot for the Temkin adsorption isotherm (Figure 8c) suggests that the

Table 4. Kinetic Parameters for Adsorption of the MB Dye onto RC-nZVI

	concentration ($mg \cdot L^{-1}$)				
parameter	25	50	100	150	200
$q_{e,exp}$ ($mg \cdot g^{-1}$)	8.10	15.46	30.40	43.33	53.16
pseudo-first-order					
$q_{e,cal}$ ($mg \cdot g^{-1}$)	8.78	18.14	31.16	39.10	55.76
K_1 (min^{-1})	0.046	0.033	0.035	0.027	0.019
R^2	0.988	0.975	0.971	0.961	0.961
(χ^2)	0.944				
pseudo-second-order					
$q_{e,cal}$ ($mg \cdot g^{-1}$)	15.34	28.18	43.22	66.46	155.4
K_2 ($mg \cdot g^{-1}$)	0.0038	0.0021	0.0012	0.0014	0.0002
R^2	0.907	0.949	0.970	0.910	0.831
(χ^2)	34.529				
Elovich					
β ($g \cdot mg^{-1}$)	0.328	0.171	0.102	0.103	0.050
α ($mg \cdot g \cdot min^{-1}$)	0.575	1.612	2.393	2.92	5.779
R^2	0.944	0.961	0.970	0.920	0.918

https://doi.org/10.1021/acsomega.1c03355
ACS Omega 2021, 6, 25397−25411

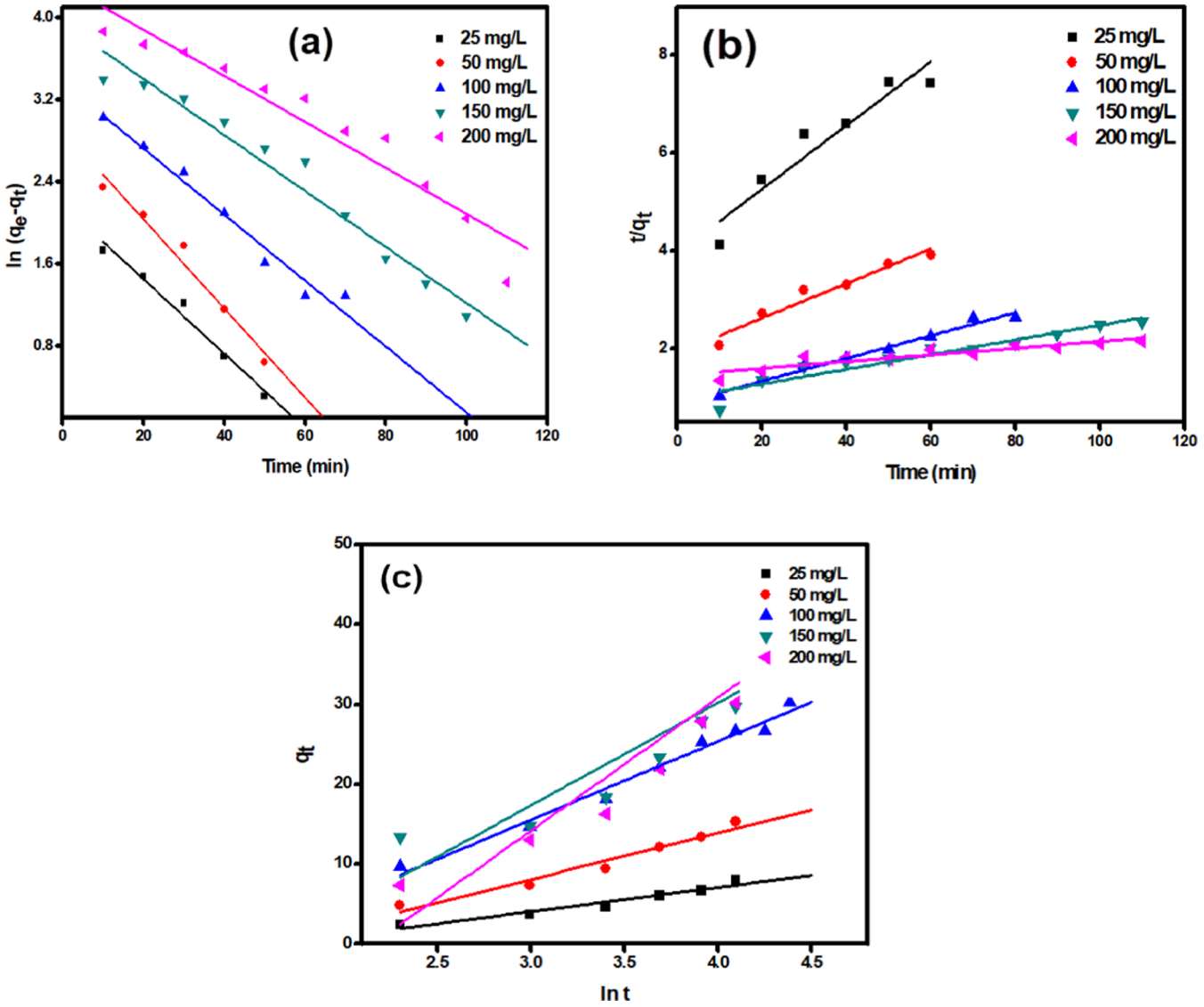

Figure 7. Adsorption kinetic models: (a) pseudo-first-order, (b) pseudo-second-order, and (c) Elovich model.

adsorption of MB onto RC-nZVI is physical adsorption, since the value of b is less than 82 KJ mol^{-1}.[93]

2.3.3. Comparison with the Reported Green-Synthesized nZVI. To evaluate the potentiality of the synthesized RC-nZVI as an adsorbent, its adsorption capacity in the removal process of MB was compared with those of the reported green-synthesized nZVI adsorbents. It is obvious from Table 6 that RC-nZVI has a good adsorption capacity towards MB and hence can be applied as a green and clean adsorbent for the treatment of cationic dyes from wastewater.

2.3.4. Mechanism of MB Removal onto RC-nZVI. Figure 9 shows the proposed mechanism for the removal of MB onto RC-nZVI. MB removal by RC-nZVI can proceed via different pathways, including the following:

(i) Adsorption of MB particles onto RC-nZVI via electrostatic interaction between the cationic MB dye molecules and the negatively charged RC-nZVI (ZP of −14.9 mV), as clarified from ZP measurements.

(ii) Degradation that takes place firstly via MB adsorption on RC-nZVI, followed by reductive cleavage of MB molecules to mineralization products.[99] The electrons produced from the oxidation of Fe^0 are utilized in the reduction of MB dye, causing decolorization (eq 1 and 24).[100]

$$Fe^0 \rightarrow Fe^{2+} + 2e^- \quad (1)$$

$$MB + ne^- \rightarrow CO_2 + H_2O + \text{minerlization products} \quad (2)$$

Moreover, Fe^0 forms H_2O_2 in the presence of O_2 and H^+ (eq 3), which produces reactive $^{\bullet}OH$ radicals (eq 4).[101] $^{\bullet}OH$ radicals are strong oxidants of organic dyes, which is responsible for decolorization (eq 5).[102]

$$Fe^0 + O_2 + 2H^+ \rightarrow Fe^{2+} + H_2O_2 \quad (3)$$

$$Fe^{2+} + H_2O_2 \rightarrow Fe^{3+} + {}^{\bullet}OH + OH^- \quad (4)$$

$$MB + {}^{\bullet}OH \rightarrow {}^{\bullet}OH + CO_2 + H_2O + \text{minerlization products} \quad (5)$$

(iii) Formation of Fe^{2+}/Fe^{3+} ion−MB complexes as a result of MB precipitation due to the combination with Fe^{2+}, and Fe^{3+} that is produced from the further oxidation of Fe^{2+} according to eq 3.[103]

https://doi.org/10.1021/acsomega.1c03355
ACS Omega 2021, 6, 25397−25411

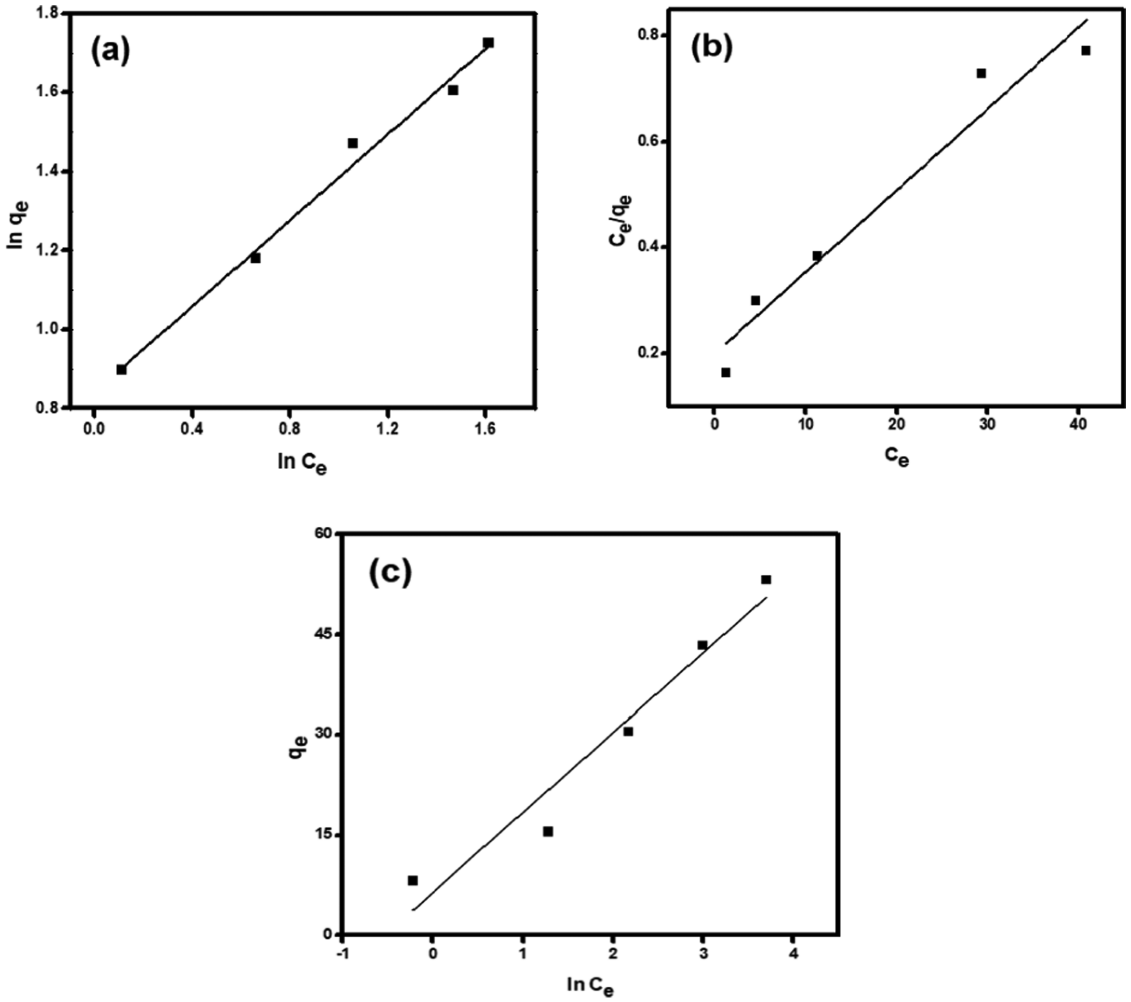

Figure 8. Adsorption models: Langmuir (a), Freundlich (b), and Temkin (c) for adsorption of the MB dye onto RC-nZVI.

Table 5. Adsorption isotherm parameters for the adsorption of MB dye onto RC-nZVI

isotherm model	parameter	value
Langmuir	q_m (mg·g^{-1})	61.73
	K_L (L·mg^{-1})	0.092
	R_L	0.259
	R^2	0.950
Freundlich	K_F (L·mg^{-1})	2.321
	n	1.838
	R^2	0.990
Temkin	B (J·mol^{-1})	207.55
	B (KJ·mol^{-1})	0.207
	A	1.708
	R^2	0.950

Table 6. Comparison of the Maximum Adsorption Capacity (q_m) of RC-nZVI with Those of Other Reported nZVI Adsorbents[a]

adsorbent	pollutant	q_m (mg·g^{-1})	ref
nZVI (using sweet lime pulp)	MB	14.76	85
TP-nZVI	MB	72.60	68
nZVI (liquid-phase reduction)	MB	5.53	94
nZVI (using *Platanus occidentalis*)	MB	126.60	95
nZVI	Amoxicillin	40.28	96
nZVI	Pb^{2+}	50.31	97
nZVI (using Korla fragrant)	Cr(VI)	46.62	98
RC-nZVI	MB	64.94	this study

[a]TP = Tea polyphenols.

$$2Fe^{2+} + 4H^+ + O_2 \rightarrow 4Fe^{3+} + 2H_2O \quad (6)$$

(iv) Oxidation of nZVI to Fe^{2+}, producing free electrons that easily reduce MB into colorless leuco-methylene blue[35,104] (eq 7).

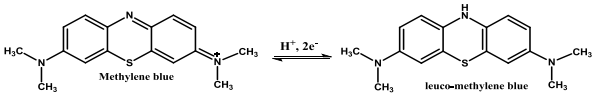

(7)

2.3.5. Reusability of nZVI. Reusability is a major factor for any adsorbent to be applicable in large-scale applications. In this contest, the synthesized RC-nZVI was tested for reuse for 5 cycles. After complete adsorption of the MB dye, RC-nZVI was easily separated by centrifugation, washed with ethanol (99%) as a desorption medium, dried in an air oven at 60 °C for 3 h, and then tested for the next adsorption run. Figure 9 shows the reusability of RC-nZVI in the removal of MB; the synthesized RC-nZVI can retain its adsorption ability (>87%) even after 5 consecutive cycles, revealing that RC-nZVI represents a green and environmentally friendly and low-cost adsorbent (Figure 10).

https://doi.org/10.1021/acsomega.1c03355
ACS Omega 2021, 6, 25397−25411

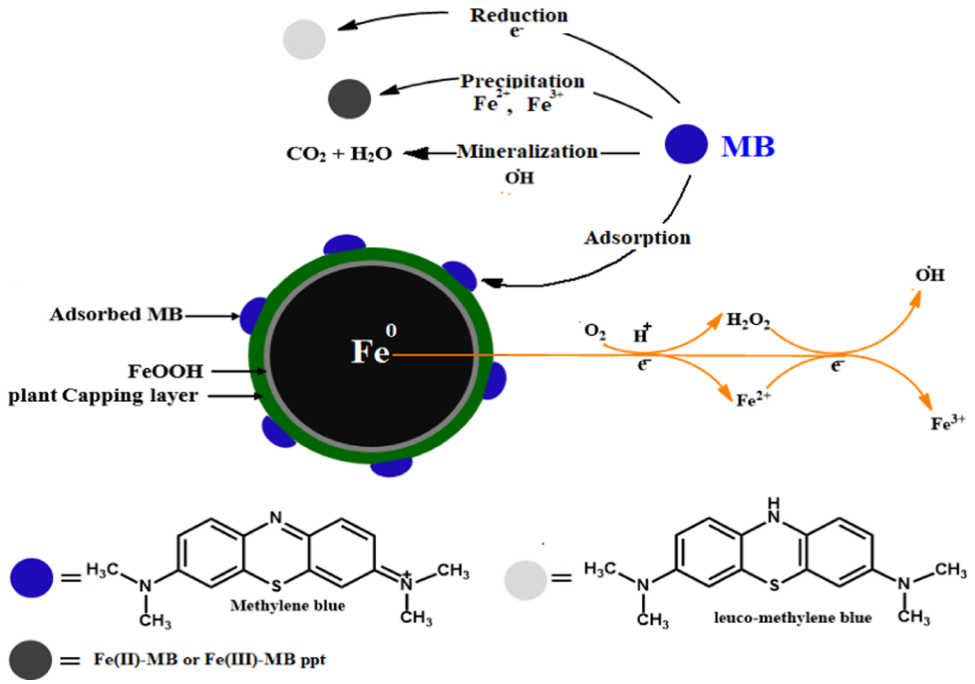

Figure 9. Proposed mechanism for the removal of MB onto RC-nZVI.

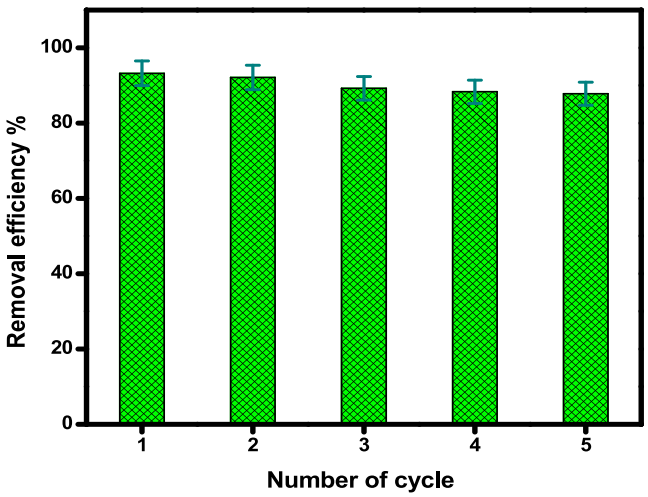

Figure 10. Reusability of RC-nZVI in MB dye adsorption.

3. CONCLUSIONS

In this work, a novel and green synthesis of nZVI was achieved by a facile and one-step method using *R. communis* seed extract. *R. communis* acts as a reducing and capping agent for nanoparticles. The biomolecules in the extract, which were determined by the phytochemical screening, reduce the aggregation of nZVI and enhance its reactivity. The phytochemical screening of the plant extract also indicated the presence of flavonoids, tannins, saponins, and phenols, which provide a synergistic effect for the reduction and stabilization of RC-nZVI. The MB removal efficiency reached a maximum of 96.8%. The regeneration efficiency was decreased to 87% after five cycles, indicating good stability and activity.

4. MATERIALS AND METHODS

4.1. Materials. All reagents used in this study were of analytical grade and used without further purification. All aqueous solutions were prepared using double-distilled water. Ferric chloride hexahydrate (97%, $FeCl_3{\cdot}6H_2O$) was purchased from Sigma-Aldrich. Ethanol (99.9%, C_2H_5OH), sodium hydroxide (97%, NaOH), and hydrochloric acid (37%, HCl) were obtained from Merck. Methylene blue (MB) dye ($C_{16}H_{18}N_3SCl$, 319.85 g mol^{-1}) was purchased from MP Bio-medical, LLC.

4.2. Preparation of Plant Extract. Fresh *R. communis* specimens were collected from different localities of the black sand area along the Mediterranean Sea Coast, Al Burullus lake, Kafr El-Shaikh, Egypt, with coordinates 31°35′30.2″N 31°05′40.7″E, during November−December 2019. The plant seeds were collected and washed using tap water and distilled water repeatedly to remove any dust and particulate matter on them. The seeds were then left in air at room temperature till they were completely dried. Afterward, specimens were shredded into small pieces using a sterilized knife before grinding by a stainless-steel mill to get a homogeneous fine powder (0.5 μm), and then kept in a dark place at room temperature for further use. A certain amount of plant seed fine powder was soaked in distilled water (5% W/V) and gently stirred at 70 °C for 20 min to get a reddish-brown extract. The extract was collected and centrifuged at 5000 rpm for 10 min, and the supernatant was filtered using Whatman filter paper number 1. Then, the resulting clear solution was stored in a clean, sterilized, and dried Falcon tube in a refrigerator at 4 °C for further use.

4.3. Phytochemical Screening of *R. communis*. Phytochemical screening of *R. communis* seeds was conducted as done by Yadav and Agarwala.[105] Table 1 shows various tests for the presence or absence of tannins, alkaloids, saponins, terpenoids, flavonoids, carbohydrates, fats and fixed oils, phenols, and anthraquinone glycosides.

4.4. Green Synthesis of nZVI. Ten milliliters of plant seed extract was added drop by drop with constant stirring to an aqueous solution of Fe^{3+} ions (5 mL, 0.05 M) in a clean sterilized flask. The resultant solution was then stirred for

https://doi.org/10.1021/acsomega.1c03355
ACS Omega 2021, 6, 25397−25411

Scheme 1. Schematic Diagram and Digital Photographs for the Green Synthesis of nZVI using RC seed extract and Removal of the MB dye (Photographs taken by Ahmed M. Abdelfatah)

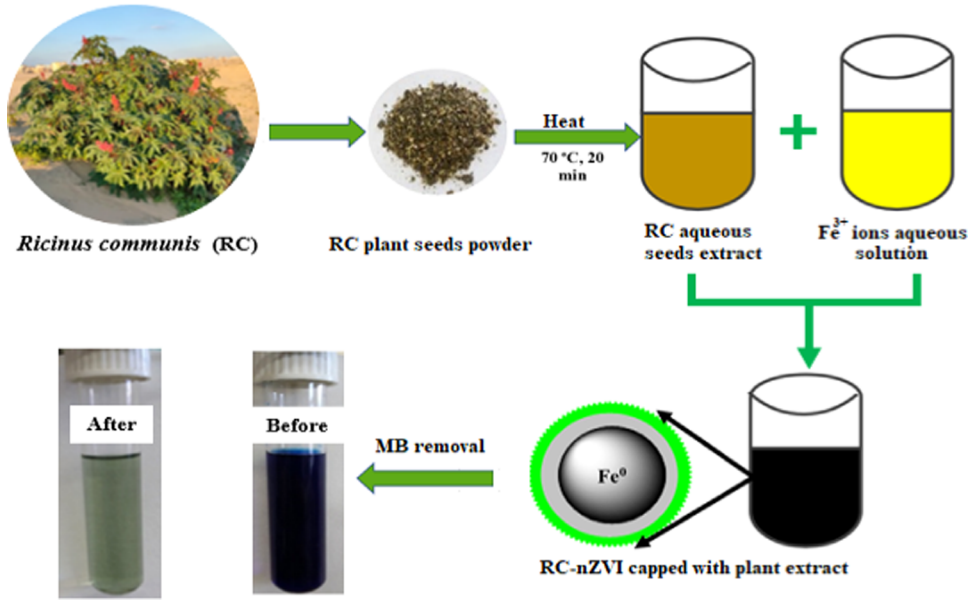

another 15 min to enhance the size distribution, followed by centrifugation at 12 000 rpm for 5 min. The obtained black product was washed three times using distilled water and ethanol and dried in an oven at 60 °C for 12 h and nominated as RC-nZVI.

Scheme 1 represents the green synthesis of RC-nZVI using the RC aqueous extract and Fe^{3+} ions for the adsorptive removal of the MB dye.

4.5. Characterization of RC-nZVI. The optical properties of the green-synthesized RC-nZVI were characterized using a double-beam UV−visible spectrophotometer (T70/T80 series UV/Vis Spectrophotometer, PG Instruments Ltd, U.K.) in the wavelength range 200−800 nm. The morphology and size distribution were determined using transmission electron microscopy (TEM) (JEM-1400 Plus instrument, operated at an accelerating voltage of 80 KV). To assess the possible functional group in the seed extract that is responsible for the reduction and stabilization process, the Fourier transform infrared (FT-IR) technique was utilized; the measurement was conducted for a ground sample with KBr on a JASCO spectrometer over the range 4000−600 cm^{-1}. The elemental analysis was performed using energy-dispersive X-ray spectroscopy (EDS) on a scanning electron microscope, JEOL model JSM-IT100. The surface charge was determined using ζ-potential (Nano-ZS90, Malvern, U.K.). To determine the crystallographic structure of nZVI powder, the XRD spectrum was recorded using an X-ray diffractometer (PXRD-6000 SHIMADZU) with a voltage of 40 KV and a current of 30 mA with Cu Kα radiation (K = 1.54056 Å) in the angle range of 10−80 °C. Furthermore, the binding energies and elemental composition of the RC-nZVI were examined by X-ray photoelectron spectroscopy (XPS, Thermo Scientific ESCALAB 250Xi VG). The particle size of RC-nZVI was determined using a zeta nanosizer (Nano-ZS90, Malvern, U.K.), equipped with a He−Ne laser (λ = 633 nm, max 5 mW) and operated at a scattering angle of 173°.

4.6. Batch Experiment. A stock solution of MB (1000 mg·L^{-1}) was prepared and kept at 25 °C in the dark. A series of diluted MB solutions (25−200 mg·L^{-1}) were prepared by dilution from the stock solution. In all, 0.03 g of RC-nZVI was added to 10 mL of MB dye solution (25 °C and pH 6) and stirred using an orbital shaker (Stuart, orbital shaker/SSL1) at 150 rpm. Sample aliquots were drawn at different time intervals (1−160 min). The residual concentration of MB was determined using a UV−visible spectrophotometer (T70/T80 series UV/Vis Spectrophotometer, PG Instruments Ltd, U.K.) equipped with a quartz cell at λ_{max} = 665 nm. The percentage removal, R%, of the MB and the amount of MB transferred onto the surface of the adsorbent, q_t (mg·g^{-1}), were calculated using the following equations.[106]

$$R(\%) = \frac{C_o - C}{C_o} \times 100 \quad (8)$$

where R (%) is the MB removal efficiency (%), and C_o and C are the concentrations of MB at time 0 and t, respectively (mg·L^{-1}), and

$$q = \frac{(C_o - C) \times V}{m} \quad (9)$$

where q is the quantity of MB adsorbed per unit mass of adsorbent (mg·g^{-1}), C_o is the initial concentration of MB, C is the concentration of MB at time t, V is the volume of the solution (L), and m is the mass of RC-nZVI (g).

AUTHOR INFORMATION

Corresponding Authors

Abdelazeem S. Eltaweil − *Department of Chemistry, Faculty of Science, Alexandria University, Alexandria 21321, Egypt;* orcid.org/0000-0001-8912-1244;
Email: abdelazeemeltaweil@alexu.edu.eg

Mohamed E. El-Khouly − *Institute of Basic and Applied Sciences, Egypt-Japan University of Science and Technology (E-JUST), New Borg El-Arab, Alexandria 21934, Egypt;*
Email: mohamed.elkhouly@ejust.edu.eg

https://doi.org/10.1021/acsomega.1c03355
ACS Omega 2021, 6, 25397−25411

Authors

Ahmed M. Abdelfatah − *Green Technology Group, Environmental Sciences Department, Faculty of Science, Alexandria University, Alexandria 21511, Egypt*

Manal Fawzy − *Green Technology Group, Environmental Sciences Department, Faculty of Science, Alexandria University, Alexandria 21511, Egypt;* orcid.org/0000-0002-9401-9049

Complete contact information is available at: https://pubs.acs.org/10.1021/acsomega.1c03355

Notes

The authors declare no competing financial interest.

■ ACKNOWLEDGMENTS

This work was financially supported by SMART WATIR, ERANETMED-3−227 project, Egyptian Academy of Scientific Research and Technology.

■ REFERENCES

(1) Li, Y.; Du, Q.; Liu, T.; Peng, X.; Wang, J.; Sun, J.; Wang, Y.; Wu, S.; Wang, Z.; Xia, Y.; Xia, L. Comparative study of methylene blue dye adsorption onto activated carbon, graphene oxide, and carbon nanotubes. *Chem. Eng. Res. Des.* **2013**, *91*, 361−368.

(2) Omer, A. M.; Abd El-Monaem, E. M.; Abd El-Latif, M. M.; El-Subruiti, G. M.; Eltaweil, A. S. Facile fabrication of novel magnetic ZIF-67 MOF@ aminated chitosan composite beads for the adsorptive removal of Cr (VI) from aqueous solutions. *Carbohydr. Polym.* **2021**, *265*, No. 118084.

(3) Hamdy, A.; Mostafa, M. K.; Nasr, M. Regression analysis and artificial intelligence for removal of methylene blue from aqueous solutions using nanoscale zero-valent iron. *Int. J. Environ. Sci. Technol.* **2019**, *16*, 357−372.

(4) Hynes, N. R. J.; Kumar, J. S.; Kamyab, H.; Sujana, J. A. J.; Al-Khashman, O. A.; Kuslu, Y.; Ene, A.; Suresh Kumar, B. Modern enabling techniques and adsorbents based dye removal with sustainability concerns in textile industrial sector -A comprehensive review. *J. Cleaner Prod.* **2020**, *272*, No. 122636.

(5) Du, M.; Yi, Q.; Ji, J.; Zhu, Q.; Duan, H.; Xing, M.; Zhang, J. Sustainable activation of peroxymonosulfate by the Mo(IV) in MoS2 for the remediation of aromatic organic pollutants. *Chin. Chem. Lett.* **2020**, *31*, 2803−2808.

(6) Yan, Q.; Lian, C.; Huang, K.; Liang, L.; Yu, H.; Yin, P.; Zhang, J.; Xing, M. Constructing an Acidic Microenvironment by MoS2 in Heterogeneous Fenton Reaction for Pollutant Control. *Angew. Chem.* **2021**, *133*, 17292−17300.

(7) Ji, J.; Yan, Q.; Yin, P.; Mine, S.; Matsuoka, M.; Xing, M. Defects on CoS2− x: Tuning Redox Reactions for Sustainable Degradation of Organic Pollutants. *Angew. Chem.* **2021**, *133*, 2939−2944.

(8) Li, X.; Zhang, M.; Liu, Y.; Li, X.; Liu, Y.; Hua, R.; He, C. Removal of U(VI) in aqueous solution by nanoscale zero-valent iron (nZVI). *Water Qual., Exposure Health* **2013**, *5*, 31−40.

(9) Lellis, B.; Fávaro-Polonio, C. Z.; Pamphile, J. A.; Polonio, J. C. Effects of textile dyes on health and the environment and bioremediation potential of living organisms. *Biotechnol. Res. Innovation* **2019**, *3*, 275−290.

(10) Chen, D.; Zeng, Z.; Zeng, Y.; Zhang, F.; Wang, M. Removal of methylene blue and mechanism on magnetic γ-Fe2O3/SiO2 nanocomposite from aqueous solution. *Water Resour. Ind.* **2016**, *15*, 1−13.

(11) Hosny, M.; Fawzy, M.; Abdelfatah, A. M.; Fawzy, E. E.; Eltaweil, A. S. Comparative study on the potentialities of two halophytic species in the green synthesis of gold nanoparticles and their anticancer, antioxidant and catalytic efficiencies. *Adv. Powder Technol.* **2021**, *32*, 3220−3233.

(12) Eltaweil, A. S.; Abd El-Monaem, E. M.; El-Subruiti, G. M.; Abd El-Latif, M. M.; Omer, A. M. Fabrication of UiO-66/MIL-101 (Fe) binary MOF/carboxylated-GO composite for adsorptive removal of methylene blue dye from aqueous solutions. *RSC Adv.* **2020**, *10*, 19008−19019.

(13) Agarwal, S.; Tyagi, I.; Gupta, V. K.; Ghasemi, N.; Shahivand, M.; Ghasemi, M. Kinetics, equilibrium studies and thermodynamics of methylene blue adsorption on Ephedra strobilacea saw dust and modified using phosphoric acid and zinc chloride. *J. Mol. Liq.* **2016**, *218*, 208−218.

(14) Eltaweil, A. S.; Elshishini, H. M.; Ghatass, Z. F.; Elsubruiti, G. M. Ultra-high adsorption capacity and selective removal of Congo red over aminated graphene oxide modified Mn-doped UiO-66 MOF. *Powder Technol.* **2021**, *379*, 407−416.

(15) El-Subruiti, G.; Eltaweil, A.; Sallam, S. Synthesis of active MFe2O4/γ-Fe2O3 nanocomposites (metal= Ni or Co) for reduction of nitro-containing pollutants and methyl orange degradation. *Nano* **2019**, *14*, No. 1950125.

(16) Omer, A. M.; Khalifa, R. E.; Tamer, T. M.; Ali, A. A.; Ammar, Y. A.; Eldin, M. S. M. Kinetic and thermodynamic studies for the sorptive removal of crude oil spills using a low-cost chitosan-poly (butyl acrylate) grafted copolymer. *Desalin. Water Treat.* **2020**, *192*, 213−225.

(17) El-Monaem, E. M. A.; El-Latif, M. M. A.; Eltaweil, A. S.; El-Subruiti, G. M. Cobalt nanoparticles supported on reduced amine-functionalized graphene oxide for catalytic reduction of nitroanilines and organic dyes. *Nano* **2021**, *16*, No. 2150039.

(18) Sallam, S.; El-Subruiti, G.; Eltaweil, A. Facile synthesis of Ag−γ-Fe2O3 superior nanocomposite for catalytic reduction of nitro-aromatic compounds and catalytic degradation of methyl orange. *Catal. Lett.* **2018**, *148*, 3701−3714.

(19) Cheng, M.; Zeng, G.; Huang, D.; Lai, C.; Xu, P.; Zhang, C.; Liu, Y. Hydroxyl radicals based advanced oxidation processes (AOPs) for remediation of soils contaminated with organic compounds: a review. *Chem. Eng. J.* **2016**, *284*, 582−598.

(20) Deka, P.; Hazarika, A.; Deka, R. C.; Bharali, P. Influence of CuO morphology on the enhanced catalytic degradation of methylene blue and methyl orange. *RSC Adv.* **2016**, *6*, 95292−95305.

(21) Eltaweil, A. S.; El-Monaem, E. M. A.; Mohy-Eldin, M. S.; Omer, A. M. Fabrication of attapulgite/magnetic aminated chitosan composite as efficient and reusable adsorbent for Cr (VI) ions. *Sci. Rep.* **2021**, *11*, No. 16598.

(22) El-Borady, O. M.; Fawzy, M.; Hosny, M. Antioxidant, anticancer and enhanced photocatalytic potentials of gold nanoparticles biosynthesized by common reed leaf extract. *Appl. Nanosci.* **2021**, DOI: 10.1007/s13204-021-01776-w.

(23) Mohy Eldin, M. S.; Omer, A.; Soliman, E.; Hassan, E. Superabsorbent polyacrylamide grafted carboxymethyl cellulose pH sensitive hydrogel: I. Preparation and characterization. *Desalin. Water Treat.* **2013**, *51*, 3196−3206.

(24) El-Sayed, E.; Tamer, T.; Omer, A.; Mohy Eldin, M. Development of novel chitosan schiff base derivatives for cationic dye removal: methyl orange model. *Desalin. Water Treat.* **2016**, *57*, 22632−22645.

(25) Elashery, S. E.; Attia, N. F.; Omar, M.; Tayea, H. M. Cost-effective and green synthesized electroactive nanocomposite for high selective potentiometric determination of clomipramine hydrochloride. *Microchem. J.* **2019**, *151*, No. 104222.

(26) Attia, N. F.; Park, J.; Oh, H. Facile tool for green synthesis of graphene sheets and their smart free-standing UV protective film. *Appl. Surf. Sci.* **2018**, *458*, 425−430.

(27) Puthukkara P, A. R.; Jose T, S.; lal S, D. Plant mediated synthesis of zero valent iron nanoparticles and its application in water treatment. *J. Environ. Chem. Eng.* **2021**, *9*, No. 104569.

(28) Bao, T.; Damtie, M. M.; Hosseinzadeh, A.; Wei, W.; Jin, J.; Phong Vo, H. N.; Ye, J. S.; Liu, Y.; Wang, X. F.; Yu, Z. M.; Chen, Z. J.; Wu, K.; Frost, R. L.; Ni, B.-J. Bentonite-supported nano zero-valent iron composite as a green catalyst for bisphenol A degradation: Preparation, performance, and mechanism of action. *J. Environ. Manage.* **2020**, *260*, No. 110105.

(29) Xiao, C.; Li, H.; Zhao, Y.; Zhang, X.; Wang, X. Green synthesis of iron nanoparticle by tea extract (polyphenols) and its selective removal of cationic dyes. *J. Environ. Manage.* **2020**, *275*, No. 111262.
(30) Li, Z.; Xu, S.; Xiao, G.; Qian, L.; Song, Y. Removal of hexavalent chromium from groundwater using sodium alginate dispersed nano zero-valent iron. *J. Environ. Manage.* **2019**, *244*, 33−39.
(31) Lin, Z.; Weng, X.; Owens, G.; Chen, Z. Simultaneous removal of Pb(II) and rifampicin from wastewater by iron nanoparticles synthesized by a tea extract. *J. Cleaner Prod.* **2020**, *242*, No. 118476.
(32) Pirsaheb, M.; Moradi, S.; Shahlaei, M.; Wang, X.; Farhadian, N. A new composite of nano zero-valent iron encapsulated in carbon dots for oxidative removal of bio-refractory antibiotics from water. *J. Cleaner Prod.* **2019**, *209*, 1523−1532.
(33) Ai, Z.; Gao, Z.; Zhang, L.; He, W.; Yin, J. J. Core−Shell Structure Dependent Reactivity of Fe@Fe2O3 Nanowires on Aerobic Degradation of 4-Chlorophenol. *Environ. Sci. Technol.* **2013**, *47*, 5344−5352.
(34) Xu, J.-h.; Gao, N.-y.; Zhao, D.-y.; Yin, D.-q.; Zhang, H.; Gao, Y.-q.; Shi, W. Comparative study of nano-iron hydroxide impregnated granular activated carbon (Fe−GAC) for bromate or perchlorate removal. *Sep. Purif. Technol.* **2015**, *147*, 9−16.
(35) Eltaweil, A.; Mohamed, H. A.; Abd El-Monaem, E. M.; El-Subruiti, G. Mesoporous magnetic biochar composite for enhanced adsorption of malachite green dye: Characterization, adsorption kinetics, thermodynamics and isotherms. *Adv. Powder Technol.* **2020**, *31*, 1253−1263.
(36) Shubair, T.; Eljamal, O.; Khalil, A. M. E.; Tahara, A.; Matsunaga, N. Novel application of nanoscale zero valent iron and bimetallic nano-Fe/Cu particles for the treatment of cesium contaminated water. *J. Environ. Chem. Eng.* **2018**, *6*, 4253−4264.
(37) Dai, Y.; Hu, Y.; Jiang, B.; Zou, J.; Tian, G.; Fu, H. Carbothermal synthesis of ordered mesoporous carbon-supported nano zero-valent iron with enhanced stability and activity for hexavalent chromium reduction. *J. Hazard. Mater.* **2016**, *309*, 249−258.
(38) Khatami, M.; Alijani, H. Q.; Fakheri, B.; Mobasseri, M. M.; Heydarpour, M.; Farahani, Z. K.; Khan, A. U. Super-paramagnetic iron oxide nanoparticles (SPIONs): Greener synthesis using Stevia plant and evaluation of its antioxidant properties. *J. Cleaner Prod.* **2019**, *208*, 1171−1177.
(39) Hosny, M.; Fawzy, M.; El-Borady, O. M.; Mahmoud, A. E. D. Comparative study between Phragmites australis root and rhizome extracts for mediating gold nanoparticles synthesis and their medical and environmental applications. *Adv. Powder Technol.* **2021**, *32*, 2268−2279.
(40) Stefaniuk, M.; Oleszczuk, P.; Ok, Y. S. Review on nano zerovalent iron (nZVI): From synthesis to environmental applications. *Chem. Eng. J.* **2016**, *287*, 618−632.
(41) Wang, T.; Jin, X.; Chen, Z.; Megharaj, M.; Naidu, R. Green synthesis of Fe nanoparticles using eucalyptus leaf extracts for treatment of eutrophic wastewater. *Sci. Total Environ.* **2014**, *466-467*, 210−213.
(42) Zhu, M.; Wang, X.; Yang, J.; Liu, H.; Ma, J. Study on the physicochemical properties of poly(methylmethacrylate) (PMMA) modified Pd/Fe nanocomposites: Roles of PMMA and PMMA/ethanol. *Appl. Surf. Sci.* **2013**, *282*, 851−861.
(43) Zhu, F.; Ma, S.; Liu, T.; Deng, X. Green synthesis of nano zero-valent iron/Cu by green tea to remove hexavalent chromium from groundwater. *J. Cleaner Prod.* **2018**, *174*, 184−190.
(44) Vijayaraghavan, K.; Ashokkumar, T. Plant-mediated biosynthesis of metallic nanoparticles: A review of literature, factors affecting synthesis, characterization techniques and applications. *J. Environ. Chem. Eng.* **2017**, *5*, 4866−4883.
(45) Hosny, M.; Fawzy, M. Instantaneous phytosynthesis of gold nanoparticles via Persicaria salicifolia leaf extract, and their medical applications. *Adv. Powder Technol.* **2021**, *32*, 2891−2904.
(46) Dhuper, S.; Panda, D.; Nayak, P. Green synthesis and characterization of zero valent iron nanoparticles from the leaf extract of *Mangifera indica*. *Nano Trends: J. Nanotech. App.* **2012**, *13*, 16−22.
(47) Rashtbari, Y.; Hazrati, S.; Azari, A.; Afshin, S.; Fazlzadeh, M.; Vosoughi, M. A novel, eco-friendly and green synthesis of PPAC-ZnO and PPAC-nZVI nanocomposite using pomegranate peel: Cephalexin adsorption experiments, mechanisms, isotherms and kinetics. *Adv. Powder Technol.* **2020**, *31*, 1612−1623.
(48) Fazlzadeh, M.; Rahmani, K.; Zarei, A.; Abdoallahzadeh, H.; Nasiri, F.; Khosravi, R. A novel green synthesis of zero valent iron nanoparticles (NZVI) using three plant extracts and their efficient application for removal of Cr (VI) from aqueous solutions. *Adv. Powder Technol.* **2017**, *28*, 122−130.
(49) Jena, J.; Gupta, A. K. *Ricinus communis* Linn: a phytopharmacological review. *Int. J. Pharm. Pharm. Sci.* **2012**, *4*, 25−29.
(50) Dauthal, P.; Mukhopadhyay, M. Noble metal nanoparticles: plant-mediated synthesis, mechanistic aspects of synthesis, and applications. *Ind. Eng. Chem. Res.* **2016**, *55*, 9557−9577.
(51) Ovais, M.; Raza, A.; Naz, S.; Islam, N. U.; Khalil, A. T.; Ali, S.; Khan, M. A.; Shinwari, Z. K. Current state and prospects of the phytosynthesized colloidal gold nanoparticles and their applications in cancer theranostics. *Appl. Microbiol. Biotechnol.* **2017**, *101*, 3551−3565.
(52) Ovais, M.; Ayaz, M.; Khalil, A. T.; Shah, S. A.; Jan, M. S.; Raza, A.; Shahid, M.; Shinwari, Z. K. HPLC-DAD finger printing, antioxidant, cholinesterase, and α-glucosidase inhibitory potentials of a novel plant Olax nana. *BMC Complementary Altern. Med.* **2018**, *18*, No. 1.
(53) Ayaz, M.; Junaid, M.; Ullah, F.; Subhan, F.; Sadiq, A.; Ali, G.; Ovais, M.; Shahid, M.; Ahmad, A.; Wadood, A.; et al. Anti-Alzheimer's studies on β-sitosterol isolated from Polygonum hydropiper L. *Front. Pharmacol.* **2017**, *8*, 697.
(54) Ovais, M.; Khalil, A. T.; Raza, A.; Islam, N. U.; Ayaz, M.; Saravanan, M.; Ali, M.; Ahmad, I.; Shahid, M.; Shinwari, Z. K. Multifunctional theranostic applications of biocompatible green-synthesized colloidal nanoparticles. *Appl. Microbiol. Biotechnol.* **2018**, *102*, 4393−4408.
(55) Rana, A.; Kumari, N.; Tyagi, M.; Jagadevan, S. Leaf-extract mediated zero-valent iron for oxidation of Arsenic (III): Preparation, characterization and kinetics. *Chem. Eng. J.* **2018**, *347*, 91−100.
(56) Sunardi, A.; Rahardjo, S. Green synthesis and characterization of nano zero valent iron using banana peel extract. *J. Environ. Earth Sci.* **2017**, *7*, 80−84.
(57) Saif, S.; Tahir, A.; Chen, Y. Green Synthesis of Iron Nanoparticles and Their Environmental Applications and Implications. *Nanomaterials* **2016**, *6*, 209.
(58) Sravanthi, K.; Ayodhya, D.; Swamy, P. Y. Green synthesis, characterization and catalytic activity of 4-nitrophenol reduction and formation of benzimidazoles using bentonite supported zero valent iron nanoparticles. *Mater. Sci. Energy Technol.* **2019**, *2*, 298−307.
(59) Mystrioti, C.; Xanthopoulou, T.; Tsakiridis, P.; Papassiopi, N.; Xenidis, A. Comparative evaluation of five plant extracts and juices for nanoiron synthesis and application for hexavalent chromium reduction. *Sci. Total Environ.* **2016**, *539*, 105−113.
(60) Bolade, O. P.; Williams, A. B.; Benson, N. U. Green synthesis of iron-based nanomaterials for environmental remediation: A review. *Environ. Nanotechnol. Monit. Manage.* **2020**, *13*, No. 100279.
(61) Pattanayak, M.; Nayak, P. L. Green Synthesis and Characterization of Zero Valent Iron Nanoparticles from the Leaf Extract of *Azadirachta indica* (Neem). *World J. Nano Sci. Technol.* **2013**, *2*, 06−09.
(62) Somchaidee, P.; Tedsree, K. Green synthesis of high dispersion and narrow size distribution of zero-valent iron nanoparticles using guava leaf (*Psidium guajava* L) extract. *Adv. Nat. Sci.: Nanosci. Nanotechnol.* **2018**, *9*, No. 035006.
(63) Eslami, S.; Ebrahimzadeh, M. A.; Biparva, P. Green synthesis of safe zero valent iron nanoparticles by *Myrtus communis* leaf extract as an effective agent for reducing excessive iron in iron-overloaded mice, a thalassemia model. *RSC Adv.* **2018**, *8*, 26144−26155.

https://doi.org/10.1021/acsomega.1c03355
ACS Omega 2021, 6, 25397−25411

(64) Darroudi, M.; Ahmad, M. B.; Zamiri, R.; Zak, A. K.; Abdullah, A. H.; Ibrahim, N. A. Time-dependent effect in green synthesis of silver nanoparticles. *Int. J. Nanomed.* **2011**, *6*, 677−681.
(65) Lin, D.; Hu, L.; Lo, I. M. C.; Yu, Z. Size Distribution and Phosphate Removal Capacity of Nano Zero-Valent Iron (nZVI): Influence of pH and Ionic Strength. *Water* **2020**, *12*, 2939.
(66) Sharma, D.; Kanchi, S.; Bisetty, K. Biogenic synthesis of nanoparticles: A review. *Arabian J. Chem.* **2019**, *12*, 3576−3600.
(67) Shahwan, T.; Sirriah, S. A.; Nairat, M.; Boyacı, E.; Eroğlu, A. E.; Scott, T. B.; Hallam, K. R. Green synthesis of iron nanoparticles and their application as a Fenton-like catalyst for the degradation of aqueous cationic and anionic dyes. *Chem. Eng. J.* **2011**, *172*, 258−266.
(68) Wang, X.; Wang, A.; Ma, J.; Fu, M. Facile green synthesis of functional nanoscale zero-valent iron and studies of its activity toward ultrasound-enhanced decolorization of cationic dyes. *Chemosphere* **2017**, *166*, 80−88.
(69) Soliemanzadeh, A.; Fekri, M. Synthesis of clay-supported nanoscale zero-valent iron using green tea extract for the removal of phosphorus from aqueous solutions. *Chin. J. Chem. Eng.* **2017**, *25*, 924−930.
(70) Bankar, A.; Joshi, B.; Kumar, A. R.; Zinjarde, S. Banana peel extract mediated novel route for the synthesis of silver nanoparticles. *Colloids Surf., A* **2010**, *368*, 58−63.
(71) Tantra, R.; Schulze, P.; Quincey, P. Effect of nanoparticle concentration on zeta-potential measurement results and reproducibility. *Particuology* **2010**, *8*, 279−285.
(72) Nayak, D.; Ashe, S.; Rauta, P. R.; Kumari, M.; Nayak, B. Bark extract mediated green synthesis of silver nanoparticles: evaluation of antimicrobial activity and antiproliferative response against osteosarcoma. *Mater. Sci. Eng., C* **2016**, *58*, 44−52.
(73) Chen, P.-J.; Tan, S.-W.; Wu, W.-L. Stabilization or oxidation of nanoscale zerovalent iron at environmentally relevant exposure changes bioavailability and toxicity in medaka fish. *Environ. Sci. Technol.* **2012**, *46*, 8431−8439.
(74) Li, S.; Wang, W.; Liang, F.; Zhang, W.-x. Heavy metal removal using nanoscale zero-valent iron (nZVI): Theory and application. *J. Hazard. Mater.* **2017**, *322*, 163−171.
(75) Ahmad, M.; Ahmad, M.; Usman, A. R.; Al-Faraj, A. S.; Abduljabbar, A. S.; Al-Wabel, M. I. Biochar composites with nano zerovalent iron and eggshell powder for nitrate removal from aqueous solution with coexisting chloride ions. *Environ. Sci. Pollut. Res.* **2018**, *25*, 25757−25771.
(76) El Bestawy, E.; El-Shatby, B. F.; Eltaweil, A. S. Integration between bacterial consortium and magnetite (Fe 3 O 4) nanoparticles for the treatment of oily industrial wastewater. *World J. Microbiol. Biotechnol.* **2020**, *36*, No. 141.
(77) Devatha, C. P.; Thalla, A. K.; Katte, S. Y. Green synthesis of iron nanoparticles using different leaf extracts for treatment of domestic waste water. *J. Cleaner Prod.* **2016**, *139*, 1425−1435.
(78) Tamer, T. M.; Omer, A. M.; Hassan, M. A.; Hassan, M. E.; Sabet, M. M.; Eldin, M. M. Development of thermo-sensitive poly N-isopropyl acrylamide grafted chitosan derivatives. *J. Appl. Pharm. Sci.* **2015**, *5*, 1−6.
(79) Jafari, K.; Heidari, M.; Rahmanian, O. Wastewater treatment for Amoxicillin removal using magnetic adsorbent synthesized by ultrasound process. *Ultrason. Sonochem.* **2018**, *45*, 248−256.
(80) Fuente, E.; Menéndez, J.; Díez, M.; Suárez, D.; Montes-Morán, M. Infrared spectroscopy of carbon materials: a quantum chemical study of model compounds. *J. Phys. Chem. B* **2003**, *107*, 6350−6359.
(81) Khan, I.; Saeed, K.; Khan, I. Nanoparticles: Properties, applications and toxicities. *Arabian J. Chem.* **2019**, *12*, 908−931.
(82) Romero-González, R.; Frenich, A. G. *Applications in High Resolution Mass Spectrometry: Food Safety and Pesticide Residue Analysis*; Elsevier, 2017.
(83) Zhou, X.; Lv, B.; Zhou, Z.; Li, W.; Jing, G. Evaluation of highly active nanoscale zero-valent iron coupled with ultrasound for chromium (VI) removal. *Chem. Eng. J.* **2015**, *281*, 155−163.
(84) Jaiyeola, O. O.; Chen, H.; Albadarin, A. B.; Mangwandi, C. Production of bio-waste granules and their evaluation as adsorbent for removal of hexavalent chromium and methylene blue dye. *Chem. Eng. Res. Des.* **2020**, *164*, 59−67.
(85) Sahu, N.; Rawat, S.; Singh, J.; Karri, R. R.; Lee, S.; Choi, J.-S.; Koduru, J. R. Process optimization and modeling of methylene blue adsorption using zero-valent iron nanoparticles synthesized from sweet lime pulp. *Appl. Sci.* **2019**, *9*, 5112.
(86) Pezoti, O.; Cazetta, A. L.; Souza, I. P. A. F.; Bedin, K. C.; Martins, A. C.; Silva, T. L.; Almeida, V. C. Adsorption studies of methylene blue onto ZnCl2-activated carbon produced from buriti shells (Mauritia flexuosa L.). *J. Ind. Eng. Chem.* **2014**, *20*, 4401−4407.
(87) Ahamad, K. U.; Singh, R.; Baruah, I.; Choudhury, H.; Sharma, M. R. Equilibrium and kinetics modeling of fluoride adsorption onto activated alumina, alum and brick powder. *Groundwater Sustainable Dev.* **2018**, *7*, 452−458.
(88) Boparai, H. K.; Joseph, M.; O'Carroll, D. M. Kinetics and thermodynamics of cadmium ion removal by adsorption onto nano zerovalent iron particles. *J. Hazard. Mater.* **2011**, *186*, 458−465.
(89) Eltaweil, A. S.; El-Tawil, A. M.; Abd El-Monaem, E. M.; El-Subruiti, G. M. Zero Valent Iron Nanoparticle-Loaded Nanobentonite Intercalated Carboxymethyl Chitosan for Efficient Removal of Both Anionic and Cationic Dyes. *ACS Omega* **2021**, *6*, 6348−6360.
(90) Somsesta, N.; Sricharoenchaikul, V.; Aht-Ong, D. Adsorption removal of methylene blue onto activated carbon/cellulose biocomposite films: Equilibrium and kinetic studies. *Mater. Chem. Phys.* **2020**, *240*, No. 122221.
(91) Shubair, T.; Eljamal, O.; Khalil, A. M. E.; Matsunaga, N. Multilayer system of nanoscale zero valent iron and Nano-Fe/Cu particles for nitrate removal in porous media. *Sep. Purif. Technol.* **2018**, *193*, 242−254.
(92) Azzam, A. M.; El-Wakeel, S. T.; Mostafa, B. B.; El-Shahat, M. F. Removal of Pb, Cd, Cu and Ni from aqueous solution using nano scale zero valent iron particles. *J. Environ. Chem. Eng.* **2016**, *4*, 2196−2206.
(93) Erhayem, M.; Al-Tohami, F.; Mohamed, R.; Ahmida, K. Isotherm, kinetic and thermodynamic studies for the sorption of mercury (II) onto activated carbon from Rosmarinus officinalis leaves. *Am. J. Anal. Chem.* **2015**, *06*, 1−10.
(94) Hamdy, A.; Mostafa, M. K.; Nasr, M. Zero-valent iron nanoparticles for methylene blue removal from aqueous solutions and textile wastewater treatment, with cost estimation. *Water Sci. Technol.* **2018**, *78*, 367−378.
(95) Parlayıcı, Ş.; Pehlivan, E. Fast decolorization of cationic dyes by nano-scale zero valent iron immobilized in sycamore tree seed pod fibers: kinetics and modelling study. *Int. J. Phytorem.* **2019**, *21*, 1130−1144.
(96) Ali, I.; Afshinb, S.; Poureshgh, Y.; Azari, A.; Rashtbari, Y.; Feizizadeh, A.; Hamzezadeh, A.; Fazlzadeh, M. Green preparation of activated carbon from pomegranate peel coated with zero-valent iron nanoparticles (nZVI) and isotherm and kinetic studies of amoxicillin removal in water. *Environ. Sci. Pollut. Res. Int.* **2020**, *27*, 36732−36743.
(97) Arancibia-Miranda, N.; Baltazar, S. E.; García, A.; Romero, A. H.; Rubio, M. A.; Altbir, D. Lead removal by nano-scale zero valent iron: Surface analysis and pH effect. *Mater. Res. Bull.* **2014**, *59*, 341−348.
(98) Rong, K.; Wang, J.; Zhang, Z.; Zhang, J. Green synthesis of iron nanoparticles using Korla fragrant pear peel extracts for the removal of aqueous Cr(VI). *Ecol. Eng.* **2020**, *149*, No. 105793.
(99) Crane, R. A.; Scott, T. B. Nanoscale zero-valent iron: future prospects for an emerging water treatment technology. *J. Hazard. Mater.* **2012**, *211−212*, 112−125.
(100) He, Y.; Gao, J.-F.; Feng, F.-Q.; Liu, C.; Peng, Y.-Z.; Wang, S.-Y. The comparative study on the rapid decolorization of azo, anthraquinone and triphenylmethane dyes by zero-valent iron. *Chem. Eng. J.* **2012**, *179*, 8−18.
(101) Elkady, M.; Shokry, H.; El-Sharkawy, A.; El-Subruiti, G.; Hamad, H. New insights into the activity of green supported nanoscale zero-valent iron composites for enhanced acid blue-25 dye

https://doi.org/10.1021/acsomega.1c03355
ACS Omega 2021, 6, 25397−25411

synergistic decolorization from aqueous medium. *J. Mol. Liq.* **2019**, *294*, No. 111628.
(102) Wang, K.-S.; Lin, C.-L.; Wei, M.-C.; Liang, H.-H.; Li, H.-C.; Chang, C.-H.; Fang, Y.-T.; Chang, S.-H. Effects of dissolved oxygen on dye removal by zero-valent iron. *J. Hazard. Mater.* **2010**, *182*, 886−895.
(103) Li, X.-q.; Elliott, D. W.; Zhang, W.-x. Zero-valent iron nanoparticles for abatement of environmental pollutants: materials and engineering aspects. *Crit. Rev. Solid State Mater. Sci.* **2006**, *31*, 111−122.
(104) Sun, X.; Kurokawa, T.; Suzuki, M.; Takagi, M.; Kawase, Y. Removal of cationic dye methylene blue by zero-valent iron: effects of pH and dissolved oxygen on removal mechanisms. *J. Environ. Sci. Health, Part A* **2015**, *50*, 1057−1071.
(105) Yadav, R.; Agarwala, M. Phytochemical analysis of some medicinal plants. *J. Phytol.* **2011**, *3*, 10−14.
(106) Ghaedi, M.; Heidarpour, S.; Kokhdan, S. N.; Sahraie, R.; Daneshfar, A.; Brazesh, B. Comparison of silver and palladium nanoparticles loaded on activated carbon for efficient removal of methylene blue: Kinetic and isotherm study of removal process. *Powder Technol.* **2012**, *228*, 18−25.

https://doi.org/10.1021/acsomega.1c03355
ACS Omega 2021, 6, 25397−25411